Identification of Damage Associated Molecular Patterns and Extracellular Matrix Proteins as Major Constituents of the Surface Proteome of Lung Implantable Silicone/Nitinol Devices

Gupta, Akash; Burgess, Janette K; Borghuis, Theo; de Vries, Marcel P; Kuipers, Jeroen; Permentier, Hjalmar P; Bischoff, Rainer; Slebos, Dirk-Jan; Pouwels, Simon D

Published in:
Acta Biomaterialia

DOI:
10.1016/j.actbio.2022.01.016

Publication date:
2022

Acta Biomaterialia xxx (xxxx) xxx

Contents lists available at ScienceDirect

Acta Biomaterialia

journal homepage: www.elsevier.com/locate/actbio

Full length article

Identification of damage associated molecular patterns and extracellular matrix proteins as major constituents of the surface proteome of lung implantable silicone/nitinol devices

Akash Gupta[a,b,c], Janette K. Burgess[b,c], Theo Borghuis[b], Marcel P. de Vries[d], Jeroen Kuipers[e], Hjalmar P. Permentier[d], Rainer Bischoff[d], Dirk-Jan Slebos[a,c], Simon D. Pouwels[a,b,c,1,*]

[a] University of Groningen, University Medical Center Groningen, Department of Pulmonology, Groningen, the Netherlands
[b] University of Groningen, University Medical Center Groningen, Department of Pathology & Medical Biology, Groningen, the Netherlands
[c] University of Groningen, University Medical Center Groningen, Groningen Research Institute for Asthma and COPD (GRIAC), Groningen, the Netherlands
[d] Department of Analytical Biochemistry and Interfaculty Mass Spectrometry Center, Groningen Research Institute of Pharmacy, University of Groningen, Groningen, the Netherlands
[e] Department of Biomedical Sciences of Cells and Systems, University of Groningen, University Medical Center Groningen, Groningen, the Netherlands

ARTICLE INFO

Article history:
Received 29 September 2021
Revised 23 December 2021
Accepted 7 January 2022
Available online xxx

Keywords:
Medical device
Lung
Nitinol
Silicone
Protein adsorption

ABSTRACT

Lung implantable devices have been widely adopted as mechanical interventions for a wide variety of pulmonary pathologies. Despite successful initial treatment, long-term efficacy can often be impacted by fibrotic or granulation tissue formation at the implant sites. This study aimed to explore the lung-device interface by identifying the adhered proteome on lung devices explanted from patients with severe emphysema. In this study, scanning electron microscopy is used to visualize the adhesion of cells and proteins to silicone and nitinol surfaces of explanted endobronchial valves. By applying high-resolution mass-spectrometry, the surface proteome of eight explanted valves is characterized, identifying 263 unique protein species to be mutually adsorbed on the valves. This subset is subjected to gene enrichment analysis, matched with known databases and further validated using immunohistochemistry. Enrichment analyses reveal dominant clusters of functionally-related ontology terms associated with coagulation, pattern recognition receptor signaling, immune responses, cytoskeleton organization, cell adhesion and migration. Matching results show that extracellular matrix proteins and damage-associated molecular patterns are cardinal in the formation of the surface proteome. This is the first study investigating the composition of the adhered proteome on explanted lung devices, setting the groundwork for hypothesis generation and further exploration.

Statement of significance

This is the first study investigating the composition of the adhered proteome on explanted lung devices. Lung implantable devices have been widely adopted as mechanical interventions for pulmonary pathologies. Despite successful initial treatment, long-term efficacy can often be impacted by fibrotic or granulation tissue formation around the implant sites. We identified the adhered proteome on explanted lung devices using several techniques. We identified 263 unique protein species to be mutually adsorbed on explanted lung devices. Pathway analyses revealed that these proteins are associated with coagulation, pattern recognition receptor signaling, immune responses, cytoskeleton organization, cell adhesion and migration. Furthermore, we identified that especially extracellular matrix proteins and damage-associated molecular patterns were cardinal in the formation of the surface proteome.

* Corresponding author at: Hanzeplein 1, 9713 GZ, Groningen, the Netherlands.
E-mail address: s.d.pouwels@umcg.nl (S.D. Pouwels).

[1] Twitter account name: @PouwelsScience.

https://doi.org/10.1016/j.actbio.2022.01.016
1742-7061/

1. Introduction

Since the first silicone T-tube airway stent was surgically implanted in the 1960s, lung device interventions have been widely adopted as a therapeutic modality within the field of pulmonology [1]. Successful clinical trials have allowed various compositions of stents and valves to become commercially available and integrated within the treatment protocol of pulmonary disorders [2,3]. The current generation of devices are composed of silicone, a highly durable, non-toxic and chemically inert polymer [4], often combined with medical-grade nitinol, a nickel-titanium shape memory alloy exhibiting superelasticity and high strain accommodation [5]. Implantation via a minimally-invasive endoscopic approach, makes these devices a compelling alternative to traditional surgical approaches [6]. Airway stents have a long history in the management of central airway obstructions [7], whereas coils and endobronchial one-way valves are engineered primarily for lung volume reduction procedures in patients with severe emphysema [8]. With advances in this field, the number of applications of lung implantable devices continues to grow.

Despite a successful initial treatment with stents or valves, long term efficacy can often be impacted by fibrotic or granulation tissue formation at the implant sites, causing dysfunction of the device, often requiring re-interventions (Fig. 1). Secondary to granulation tissue formation, biofilm formation, colonization and hemoptysis can occur [9]. These host responses can be present in up to 50% of patients treated with lung implantable devices [9–11].

Tissue trauma during implantation, *in vivo* mechanical injuries, and a foreign body response are all possible mechanisms through which the patient's cascade of inflammation and wound healing could be evoked [12,13]. A skewed balance from favorable tissue regeneration, remodeling, and tolerance towards chronic inflammation, implant encapsulation, and fibrosis reduces the probability of extended implant success [14]. To date, no studies have been performed investigating the biological mechanisms driving the host response to airway and lung biomaterials.

With this study, we aimed to explore the lung-device interface by characterizing the surface proteomic signature of endobronchial valves from patients with severe emphysema. We identified the adhered proteome of these devices using a discovery proteomic approach, which we further validated using surface immunohistochemistry, to investigate the potential molecular signals inducing interactions between the airway wall and the biomaterial, triggering biological responses. This study lays the groundwork for follow-up investigations of the lung-device interface, as well as the cellular and molecular mechanisms driving the host response to lung devices.

2. Materials and methods

2.1. Patient characteristics

This study included four patients that were treated with endobronchial silicone-nitinol valves (Zephyr® endobronchial valves, PulmonX Corp, CA, USA) for emphysema at the University Medical Center Groningen (UMCG), who required endobronchial valve maintenance procedures following this therapy. The study was approved by the medical ethics committee of the University Medical Center Groningen (UMCG), Groningen, The Netherlands. All subjects provided written informed consent, and the data was captured in the Breathe-NL registry (NCT02815683). Valves included in this study were explanted following collateral ventilation, local fungal infection, accidental valve migration, or granulation tissue formation (Table 1). Per subject two valves were included in our study. Implant sites were bronchoscopically imaged directly after implantation and during revision bronchoscopies.

2.2. Scanning electron microscopy and elemental analysis

Samples were fixed in a mixture of 2% glutaraldehyde and 2% paraformaldehyde in 0.1M sodium cacodylate pH7.3. A post-fixation was performed with 1% osmiumtetroxide in 0.1 M sodiumcacodylate for 30 minutes at room temperature. Samples were dehydrated with ethanol (30%-50%-70%-3 × 100%) after which the samples were incubated in a 1:1 mixture of 100% ethanol and tetramethylsilane for 10 minutes, followed by 10 minutes with pure tetramethylsilane and subsequentially airdried. Samples were glued to metal stubs using double sided carbon tape, sputter coated with 3 nm palladium/gold and imaged in a Zeiss Supra55 scanning electron microscope operated at 3 KV using the SE2 detector. Elemental analysis was carried out according to the protocol described by de Boer *et al.* (2018) [15] in the same SEM at 10 KV and the X-rays were detected using an Oxford X-Max 150 energy dispersive X-ray (EDX) detector by summing 8 frames with 50 µs pixel dwell-time. Imagemaps were generated with Oxford Aztec software at 512 × 416 pixels.

2.3. Removal and extraction of adsorbed protein layer from valves

Immediately after removal from the patient, valves were submerged in phosphate-buffered saline (PBS) and washed three times

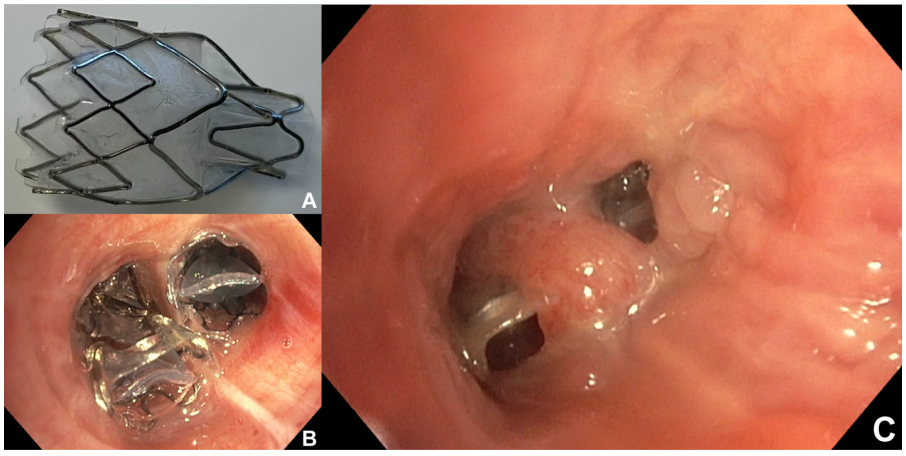

Fig. 1. Endoscopic images showing granulation tissue formation at the implant site of an emphysema patient treated with endobronchial valves. A) Image of an endobronchial valve prior to implantation. B) Endoscopic image taken directly after placement of the valves, C) Endoscopic image taken at the same position one year later.

Table 1
Patient characteristics. FEV1 (Forced Expiratory Volume), FVC (Forced Vital Capacity), RV (Residual Volume).

Patient	1	2	3	4
Length of implantation (months)	2	21	8	11
Reason for admission	Collateral ventilation	Fungi infection	Migration	Granulation tissue
Age (years)	66	60	67	69
Sex (M/F)	F	F	M	F
BMI (kg/m^2)	32	27	22	22
Smoking status (current/ex-smoker)	ex	Ex	ex	ex
FEV1 (% predicted)	37	15	28	20
FVC (% predicted)	57	48	85	68
RV (% predicted)	209	286	215	235
Inhaled corticosteroids (Y/N)	Y	Y	Y	Y
Bronchodilators (Y/N)	Y	Y	Y	Y
Mucolytics (Y/N)	N	N	N	N
Positive microbiology	Aspergillus	N	N	H. Influenzae

to remove any non-adherent tissue. Valves were decellularized through incubation at 37°C in 1 × 0.5% EDTA Trypsin for 10 min followed by a wash with PBS. Proteins were mechanically and chemically eluted from the surface through submersion in SDS sample buffer containing 62.5 mM Tris-HCl (pH 6.8), 2% sodium dodecyl sulfate (SDS), 0.002% bromophenol blue, 10% glycerol, 0.7135 M (5%) β-mercaptoethanol for 24 h in a thermomixer at 99°C with 600 rpm.

Samples were loaded on an 8 % pre-cast RunBlue gel (Expedeon), and shortly run at 100 V for 1-5 min. Gel staining was performed using InstantBlue (Expedeon) followed by a wash with ultrapure water. Coomassie-stained samples were excised in one gel slice which was further cut into small pieces and de-stained using 70% 50 mM NH_4HCO_3 and 30% acetonitrile. Reduction was performed using 10 mM dithiothreitol (DTT) dissolved in 50 mM NH_4HCO_3 for 30 min at 55°C. Next, the samples were alkylated using 55 mM iodoacetamide in 50 mM NH_4HCO_3 for 30 min at room temperature and protected from light. Subsequently, samples were washed for 10 min with 50 mM NH_4HCO_3 and for 15 min with 100% acetonitrile. The remaining fluid was removed and gel pieces were dried for 15 min at 55°C. The tryptic digest was performed by addition of sequencing-grade modified trypsin (10 ng/mL in 50 mM NH_4HCO_3) and incubation overnight at 37°C. Peptides were extracted using 5% formic acid followed by a second elution with 5% formic acid in 75% acetonitrile. Samples were dried in a SpeedVac centrifuge and dissolved in 20 µL 5% formic acid.

2.4. Qualitative LC/MS analysis

Online chromatography of peptides was performed with an Ultimate 3000 nano-HPLC system (Thermo Fisher Scientific, MA, USA) coupled online to a Q Exactive Plus mass spectrometer with a NanoFlex source (Thermo Fisher Scientific) equipped with a stainless-steel emitter. Tryptic digests were loaded onto 5 mm × 300 µm i.d. trapping micro columns at the flow rate of 20 µL/min. After loading and washing for 3 minutes, peptides were forward-flush eluted onto a 50 cm x 75 µm i.d. nanocolumn, packed with Acclaim C18 PepMAP100 2 µm particles (Thermo Fisher Scientific). The following mobile phase gradient was delivered at the flow rate of 300 nL/ min: 2–45% of acetonitrile with 0.1% formic acid in H_2O (solvent) in 90 min; 50–80% solvent in 1 min; 80% solvent during 9 min, and back to 2% solvent in 1 min and held at 2% solvent for 19 min.

Mass spectrometry (MS) data were acquired using a data-dependent top-15 method dynamically choosing the most abundant not-yet-sequenced precursor ions from the survey scans (m/z 300–1650) with a dynamic exclusion time of 20 s. Sequencing was performed via higher energy collisional dissociation (HCD) fragmentation with a target value of 2e4 ions determined with predictive automatic gain control. Isolation of precursors was performed with a window of 1.8 Da. Survey scans were acquired at a resolution of 70,000 at m/z 200. Resolution for HCD spectra was set to 17,500 at m/z 200 with a maximum ion injection time of 50 ms. Normalized collision energy was set at 28. The S-lens radio frequency (RF) level was set at 60 and the capillary temperature at 250°C. Precursor ions with single, unassigned, or six and higher charge states were excluded from fragmentation selection.

2.5. Protein identification

Raw mass spectrometry data were analyzed using PEAKS X+ (Bioinformatics Solutions Inc., Waterloo, Ontario, Canada) and matched against the Human Uniprot/Swissprot database (downloaded April 4, 2019, 20404 entries) combined with the MaxQuant contaminants database. The retrieved sets of valve specific proteome data were further processed to remove non-human proteins and contaminants that were flagged by the MaxQuant contaminants database as well as Keratins and immunoglobulins that were not-flagged.

2.6. Bioinformatic analyses

A Venn analysis was performed on the eight sets of PEAKs-derived protein lists derived from the 8 explanted valves to evaluate the intra-patient and inter-patient variability in terms of adsorbed proteins using the web-based program, InteractiVenn [16]. Intra-patient valve proteome variability was determined by carrying out a Venn analysis on the protein lists from both valves of each patient. The percentage of overlap in proteins between the two valves of each patient was calculated. The protein lists from both valves of each patient were then combined, removing duplicates, and a Venn analysis was repeated with the combined sets from each patient to evaluate the inter-patient variability in adsorbed proteins (Fig. 2). The percentage of overlap in proteins between the valves of all four patients was calculated. Finally, a list of unique protein species was created by combining the original eight sets of mass spectrometry data and removing duplicates. Proteins that were identified in at least 6 out of the 8 valves were defined as “mutually adsorbed” and compiled in a list further analysis.

Next, an unranked gene list was derived from the list of mutually adsorbed proteins. This gene list was subjected to a functional and pathway enrichment analysis to identify significantly enriched (i.e. over represented) functional categories and pathways. The web-based tool, g:Profiler, was used for these analyses with a specific search for terms and pathways from the updated resources, Gene Ontology (GO) and REACTOME [17]. The following GO categories were included: *biological process, cellular component*

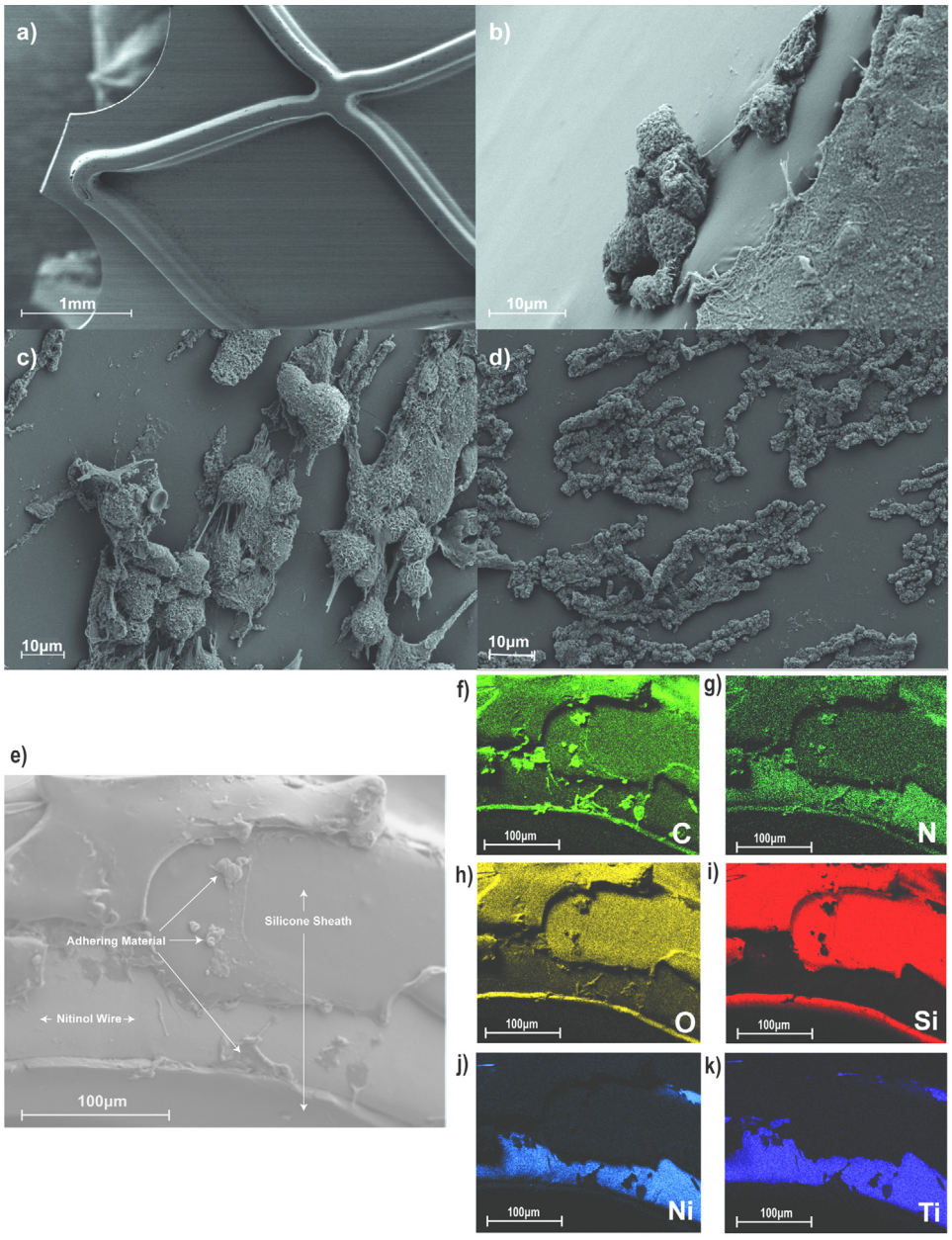

Fig. 2. Scanning electron microscope (SEM) images and elemental analysis of the surface of an explanted endobronchial valve (EBV) a) SEM image of a clean valve prior to implantation, showing the nitinol wire frame and silicone membrane b-d) SEM images of cells and organic material adhering to the explanted EBV surface. e) SEM image of an explanted endobronchial valve with x-ray mapping (f-k) of elemental Carbon (C), Nitrogen (N), and Oxygen (O) showing the adhesion of organic material and Silicone (Si), Nickel (Ni), Titanium (Ti) depicting the material exposed on the valve surface.

and *molecular function.* All GO annotations derived computationally or automatically assigned in the absence of curator review, were excluded from this analysis. A cumulative hypergeometric test was adopted to measure the gene-enrichment in annotation terms, followed by a correction for multiple testing using the g:Profilers default g:SCS (sets Count and Sizes) method [17].

The biological process and REACTOME enrichment analyses results were further analyzed and visualized according to the protocol described by Reimand *et al.* (2019) [18]. Terms with a size smaller than 5 or greater than 350 genes were excluded to improve the interpretation of less concentrated biological pathways. Enrichments were mapped using the Cytoscape desktop program (v3.8.2) [19] based EnrichmentMap Pipeline Collection (v1.1.1). The EnrichmentMap (v3.3.1) plugin was used to collapse redundancies and visualize the commonly enriched pathways in a network layout [20]. The enrichment results were mapped as a network of gene-sets (nodes), representing statistically significant terms and enriched genes, and connections (edges), representing the degree of overlap of genes between gene-sets. Next, using the clusterMaker2 (v1.3.1) [21] and AutoAnnotate plugin (v1.3) [22] the gene-sets were grouped into clusters by applying the Markov cluster (MCL) algorithm, based on the edge weights of their similarity coefficients. The clusters were automatically annotated using the WordCloud algorithm (v3.1.3) [23]. Annotations were manually adjusted to better represent the incorporated gene-sets.

2.7. Matching mutual implant proteome with published datasets

Extracellular matrix (ECM) and ECM-associated gene signatures in the mutual implant proteome were identified with reference

to The Matrisome project [24]. The Matrisome project has characterized the human "matrisome", an ensemble of extracellular matrix and ECM-associated proteins. This database contains over 1000 genes coding for core ECM proteins (collagens, proteoglycans, and ECM glycoproteins) and ECM-associated proteins (ECM-regulators, secreted factors, and ECM-affiliated proteins). Furthermore, the mutual implant proteome was also matched for intracellular and extracellular damage-associated molecular patterns (DAMPs), the reference list was developed by referring to the most recent DAMP reviews [25–27].

2.8. Validation by immunohistochemistry staining

Explanted valves were submerged in PBS and washed three times to remove any non-adherent tissue. Valves were decellularized through incubation at 37°C in 1 × 0.5% EDTA Trypsin for 10 minutes, followed by a wash with PBS. Decellularized valves were fixed with 2% paraformaldehyde for 20 minutes at RT and washed with PBS. The valves were sectioned and trimmed using a wire cutter to fit in an 8-well chambered coverslips (9.4 × 10.7 × 9.3 mm^3). Sections intended for immunostaining were then blocked with 1% BSA for 30 minutes at RT. Primary and secondary antibodies were prepared with experiment-specific dilutions (see below) in 1% BSA in PBS. Following blocking, samples were incubated with the primary antibody overnight at 4°C. After 16h of incubation, samples were washed three times with 0.1% Tween/PBS and incubated with a fluorochrome-conjugated secondary antibody for 60 minutes. Following another 3 rounds of washes with 0.1% Tween/PBS, followed by one wash with PBS, immunostained valves were fitted into an 8-well borosilicate glass chambered coverslips (#1.5H µ-Slide 8 Well high glass coverslip bottom, 170 µm +/- 5µm, D263M Schott glass, 80807, Ibidi, Gräfelfing, Germany) and submerged in PBS for imaging. Image acquisition was performed using a Zeiss Cell Discover 7 microscope with bright field and fluorescent capabilities, equipped with a widefield Axiocam 506 b/w digital camera. All images were captured with consistent exposure settings and 5x or 20x objectives used in combination with a 0.5x Optovar lens to obtain a 2.5x and 10x magnification. Images were processed using FIJI [28] to generate maximal intensity Z-projections for the stacks. Primary antibodies used were rabbit anti-fibronectin (1:100; ab2413, Abcam Cambridge, England), rabbit anti-vitronectin (1:100; ab45139, Abcam), rabbit anti-S100A8 (1:100; orb48527, Biorbyt, Cambridge, England), rabbit anti-HMGB1 (1:100; GTX101277, GeneTex), rabbit IgG isotype control (1:500 GTX35035 GeneTex). The secondary antibody used was Alexa fluor-555 anti-rabbit (1:500; ab150078, Thermofischer Scientific). Three control sections were included to evaluate the specificity of the positive immunosignals. These included a section with no staining, staining with only the secondary antibody, and staining with an rabbit IgG isotype control antibody.

2.9. Statistical analyses

For the functional and pathway enrichment analyses, a cumulative hypergeometric test was adopted to measure the gene-enrichment in annotation terms, followed by a correction for multiple testing using the g:Profilers default g:SCS (sets Count and Sizes) method [17]. Results were considered statistically significant when the false discovery rate (FDR) adjusted p-value (Q-value) was $\leq$0.05. For the enrichment map, gene-sets were filtered based on their Q-value, with a threshold of $\leq$0.001, as well as their similarity score. The similarity score threshold was set at 0.375 derived from the default Jaccard-Overlap combined metric (50% Jaccard + 50% Overlap).

3. Results

3.1. Valve surface characterization

Fig. 1 depicts the formation of granulation tissue around an implanted medical device for emphysema (endobronchial valve), one year after initial implantation. The formation of granulation tissue was observed to be overgrowing, directly impairing the movement of the duck-bill valve mechanism, reducing the effectiveness of the device. We examined the surface of explanted endobronchial valves using SEM (Fig. 2). Adhesion of cellular material and a protein matrix were visible on the surface of the valves. To further characterize the surface, an elemental mapping analysis was performed. The EDX analysis exhibited the adherence of molecules containing the organic elements, Carbon (C), Nitrogen (N) and Oxygen (O) on the surface of the valves, distributed over both the Nitinol and Silicone surfaces (Fig. 2). The elemental analysis supported the adherence of cellular material visualized in the EM images. In addition to the confirmation of visible adhered organic material, the EDX analysis described a widespread organic element signal dispersed over the entire surface of the valve. The nitrogen signal, being a core component of amino acids, most likely described the distribution of adhered proteins.

3.2. Identification of proteins adsorbed on explanted endobronchial valves

Next, the proteomic signature on the surface of the valves was analyzed. The surface proteome of each valve varied greatly, with the number of unique proteins in each dataset ranging from 169 to 674 (Fig. 3a). To obtain an overview of the intra-patient and inter-patient variability a Venn analysis was carried out (Fig. 3a-b). More than 56% of the proteome overlapped between the two valves of each patient. A total of 956 unique protein species were identified from the eight valves. A total of 263 unique protein species were identified on the surface of at least 6 out of 8 valves and this list of mutually adsorbed proteins was further analyzed.

3.3. Functional annotation and matching

The 263 genes that encode for the assembled set of mutually adsorbed proteins were subjected to a gene ontology-based enrichment analysis, identifying overrepresented gene ontology functional categories and REACTOME pathways. A total of 333 *biological processes* (BP), 104 *molecular functions* (MF), 88 *cellular components* (CC) and 85 *REACTOME pathways* were found to be enriched within our input gene list. Enrichments were ranked based on their adjusted p-value; the top 20 ontology terms from each category were further evaluated (Fig. 4). All of the top 20 *BP* enrichments were associated with immune system processes, with neutrophil activity being exceptionally enriched. The top 20 *CC* annotations showed that the adhered proteome was predominantly of extracellular origin. The most highly enriched term among all the functional categories was the *CC* extracellular exosome ($7.3e10^{-134}$). A total of 209 of the 263 genes (80%) were annotated with the *CC* extracellular region term, indicating the high prevalence of extracellular proteins.

To better visualize the significantly enriched biological pathways, gene-sets from the REACTOME and *BP* enrichments were linked and clustered based on their similarity (Fig. 4). Prominent clusters identified were associated with coagulation, pattern recognition receptor (PRR) signaling, the immune response, cytoskeleton organization, cell adhesion and migration. These results were consistent with the foreign body response and the clinical observation of granulation tissue formation. Other clusters identified were associated with humoral antimicrobial responses, peptidase activity,

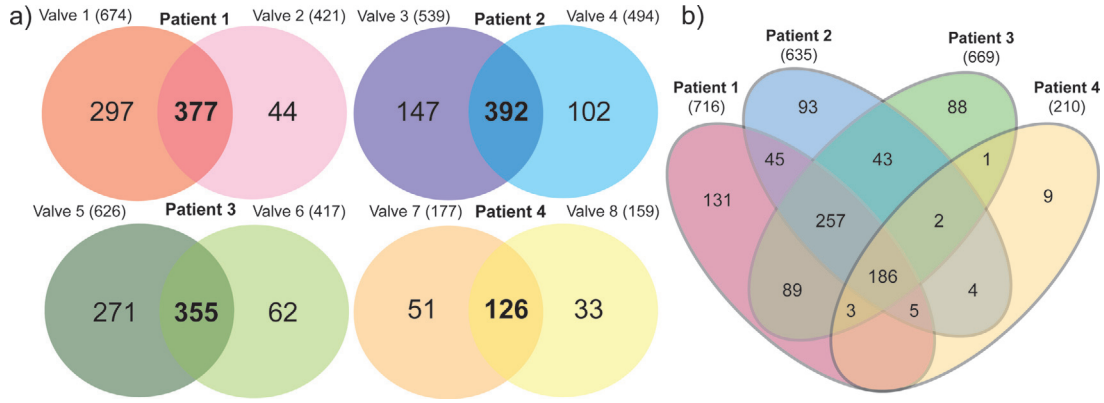

Fig. 3. Venn analysis illustrating the intra and inter-patient variability in the number of unique protein species adsorbed onto the surface of explanted endobronchial valves. (a) Venn analyses illustrating the overlap of proteins adsorbed on the two valves explanted from each patient. (b) Venn analysis illustrating the overlap of proteins between the sets of valves of each patient.

redox/oxidative stress responses, carbohydrate metabolism, ubiquitin and growth signaling.

Based on the observation of heavy extracellular protein enrichment and PRR binding/signaling, the mutual protein list was additionally matched for extracellular matrix (ECM) proteins with the matrisome classification defined by "The Matrisome Project" [24] and for DAMP proteins with reference to recent DAMP reviews [25–27]. A total of 69 unique proteins were matched, 27 ECM and ECM-associated proteins were matched from the matrisome, 27 DAMPs were from the DAMP literature, and 15 proteins from both (Fig. 5). Among this list, were core matrix proteins (fibrinogen, fibronectin and vitronectin), proteases (Cathepsins, MMPs), protease inhibitors (SERPINs), calcium binding proteins (S100s), DNA binding proteins (HMGB1, Histones), defensins (DEFA) and heat shock proteins (HSPs), indicating the importance of the fibrotic response and the host inflammatory response towards cellular damage in forming the adhered proteome on endobronchial valves.

3.4. Immunohistochemical validation of ECM and DAMP proteins

An immunohistochemical validation of the identified proteomic profiles was performed (Fig. 6). The candidate proteins, fibronectin, vitronectin, HMGB1 and S100A8 were all identified through LC/MS to be mutually adsorbed on explanted valves. These proteins were selected as representatives for the dominant ECM and DAMP protein groups identified in the mutual proteomic profile. The IgG Isotype control and secondary control demonstrated minimal, low intensity, positive immunosignals. Performing no primary or secondary staining presented a diffuse positive signal on the surface of the nitinol frame, likely due to reflection of the excitation beam. Staining of all four proteins demonstrated strong positive immunosignals on the explanted valves, a result consistent with our MS data. Positive staining was observed on both the frame and membrane surface of the valve. However, the signals for all four proteins predominantly localized to surface points on top of the nitinol frame, with an especially high prevalence at curved sections of the frame. HMGB1 and S100A8 demonstrated a dispersed puncta-like staining whereas the fibronectin and vitronectin staining were more abundant in a strand-like shape and distribution.

4. Discussion

This study was the first to analyze the adhered proteome on lung implantable medical devices. The types of proteins adhered to these devices provide important molecular cues for host inflammatory, fibrotic and foreign body reactions, potentially leading to adverse treatment effects [14]. Granulation and fibrotic tissue formation are important responses to implanted lung devices, which can compromise the device function [9–11]. Here, we showed that >40% of adhered proteins are shared between 6 out of 8 explanted endobronchial valves, indicating common biological pathways being involved in the formation of the adhered proteome of endobronchial valves. A thorough analysis of the biological pathways associated with the common adhered proteins indicated that especially ECM proteins and DAMPs are cardinal in the formation of the adhered proteome. ECM proteins are structural components of the matrix supporting cells, but are also important drivers of the wound healing and fibrotic responses, while DAMPs are molecules released upon cellular damage triggering a local inflammatory reaction. The presence of ECM proteins (Fibronectin, Vitronectin) and DAMPs (HMGB1, S100A8) was further validated using immunohistochemistry. Together, these factors may contribute to the host response of lung implantable medical devices.

Endobronchial valves are composed of a duck-bill unidirectional valve attached to a nitinol frame. All components are either composed of, or covered by silicone [29]. Silicone and nitinol have good biocompatibility profiles [5,30]. However, exposure to silicone and nitinol implants *in vivo* can evoke cellular responses leading to pathological wound healing [11,31]. A wound healing response is inevitable following implantation. Whether the response leads to favorable tissue regeneration, remodeling, and tolerance of the device or instead triggers chronic inflammation, implant encapsulation, and fibrosis is dependent on a multi-faceted interaction between the device and the unique biology of the patient [14]. A crucial mediator of this interaction is the one-of-a-kind surface proteome that develops on the surface of a device, within seconds of implantation-induced injury to local connective vascular tissue [32]. The initial layer, consisting primarily of plasma proteins, is gradually replaced through a competitive protein exchange coordinated by the physicochemical and structural properties of the biomaterial surface, the surrounding proteins, and the conditions of the microenvironment. Protein-surface interactions can also induce conformational changes in the adsorbed protein structure (e.g. α-helix loss), exposing concealed binding domains or neo-epitopes. Both the composition and conformation of the proteins adsorbed on the biomaterial surface can influence the host response by providing surface ligands for integrin-mediated anchorage of platelets and leukocytes and other resident lung cell types such as bronchial epithelial cells (source) and lung fibroblasts [14,33,47]. Integrin-mediated binding to adsorbed proteins can, through outside-in sig-

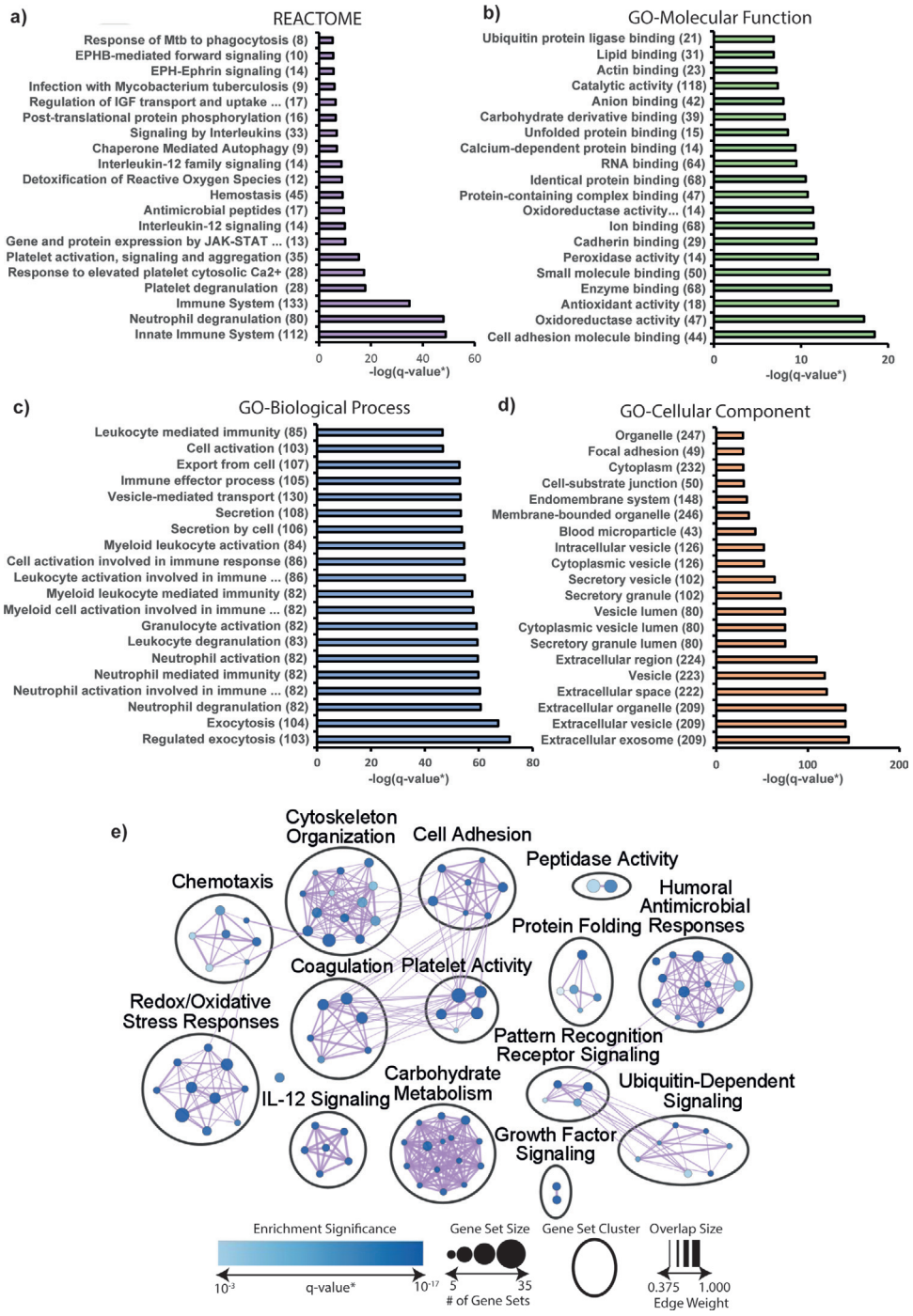

Fig. 4. Functional and pathway enrichment analysis of proteins found to be mutually adsorbed on explanted EBVs. a-d) Results from the enrichment analysis, depicting the top 20 most significant enrichments of REACTOME and Gene Ontology terms, Molecular Function, Biological Process, Cellular Component. e) An enrichment map visualization of pathway enriched gene-sets. * = FDR adjusted p-value.

naling, trigger functional response such as migration, proliferation and degranulation in many cell types [34].

Protein binding was observed on both the silicone and exposed nitinol surfaces. Silicone has a high protein-surface affinity due to its hydrophobic nature [35]. The shared proteomic profile we have assembled contains predominantly proteins found in wound healing fluid, a product of coagulation and inflammation. For most of the proteins identified, the biological relevance in influencing the host response still remains largely unknown. The degree to which each protein's influence can be described is also limited by our qualitative proteomic profiling, as some protein effects are conferred in a dose-dependent manner. Adsorbed plasma and ECM proteins including, complement 3, fibrinogen, albumin, fibronectin, and vitronectin are examples of the proteins identified in this study that readily bind to silicone [36,37] and nitinol surfaces [38]. These proteins have also been thoroughly described through *in vitro* studies to, upon adsorption, direct key components of the host response [33]. Adsorbed matrix proteins fibrinogen, fibronectin and vitronectin facilitate every stage of the foreign body response by providing surface epitopes for integrin-mediated ad-

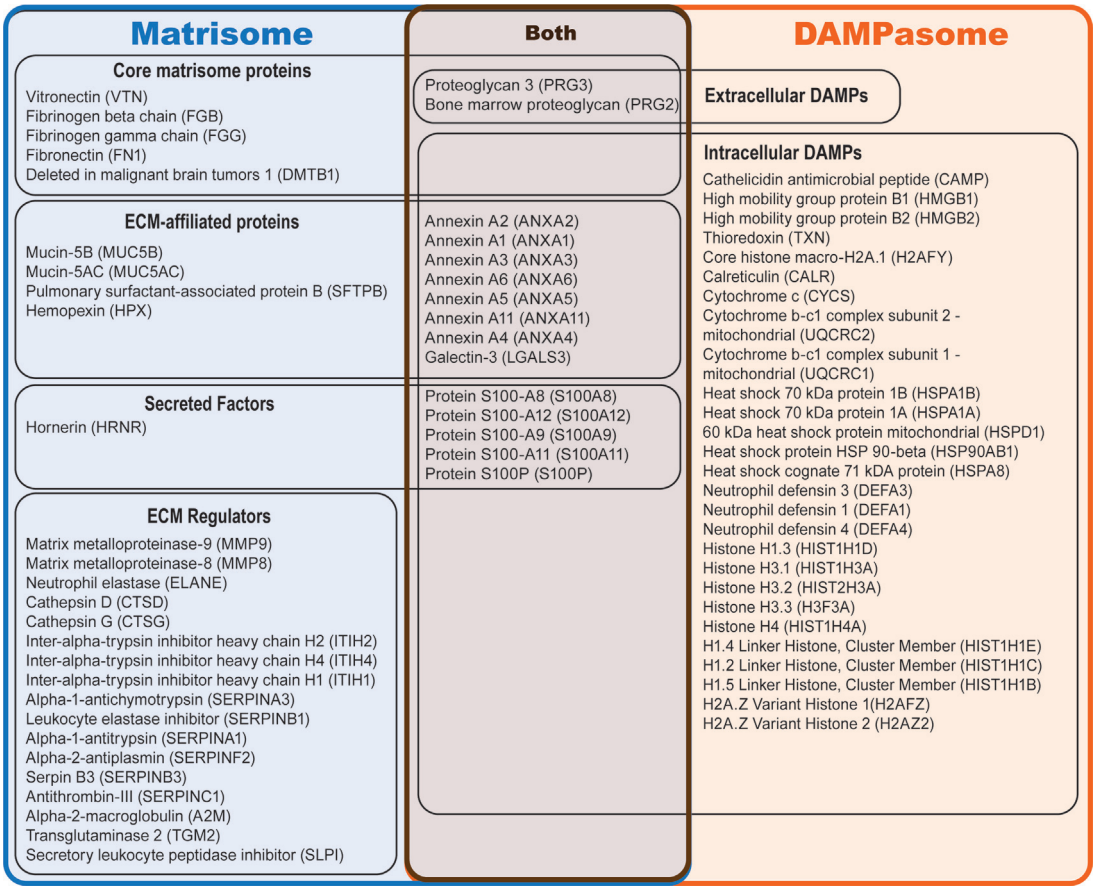

Fig. 5. List of proteins identified following matching of the proteins mutually adsorbed on explanted endobronchial valves with a Matrisome, an ensemble of extracellular matrix (ECM) and ECM-associated proteins compiled by "The Matrisome Project"[24], and extracellular and intracellular DAMPs referenced from recent DAMP reviews [25–27].

hesion and activation of platelets, neutrophils, macrophages and fibroblasts to the implant [14,33]. C3, when adsorbed, can amplify the immune response by initiating complement cascades through the alternative pathway [39]. Albumin acts as a dysopsonin, inhibiting phagocytosis and conferring a protective effect [35]. The identification of these key proteins and dominant enrichment clusters associated with coagulation, immune response and cell adhesion, suggests involvement of the surface proteome in the formation of granulation and fibrotic tissue around the valves.

A foreign body response is an expected consequence of any biomaterial intervention. [14]. However, the respiratory system presents an additional challenge for biocompatibility. Lung devices encounter the lungs' kinetic nature featuring both repetitive (e.g. breathing) and explosive motion (e.g. coughing). Next to the acute release of DAMPs upon implantation, the repetitive stress and pressure applied on the airway epithelial layer by the implanted device may induce chronic DAMP release, sustaining a local inflammatory response, potentially leading to granulation tissue formation. Several DAMPs were identified to be deposited on the valves, including high-mobility group box 1 (HMGB1), Cathelicidin antimicrobial peptide (CAMP/LL-37), and S100 proteins. These DAMPs act as ligands for the receptor of advanced glycation end-products (RAGE), which was implicated in the pathophysiology of COPD [40–43]. DAMPs can activate toll-like receptors and subsequently induce NF-κB transcription factor activity, both biological processes found to be enriched in the adsorbed proteome [44]. The adherence of DAMPs is rarely discussed in literature, however, a recent *in vitro* study showed that cell-derived DAMPs, adsorbed to polymeric surfaces, strongly induced NF-κB/AP-1 transcription factor activity and pro-inflammatory cytokine secretion in macrophages through toll-like receptor signaling [45].

The valves included in this study were implanted between 2 and 21 months (2,8,11,21 months) before being explanted due to complications (Table 1). The adsorbed proteome tends to stabilize after competitive protein exchange [46]. Hence, the adhered proteins we have identified are likely to be components of a stable protein layer, continuing to influence the biological response to the implants long after the initial wound healing response. Although these proteins can trigger abnormal wound healing, the cellularization of implants is essential for gaining immune tolerance. If a degree of tolerance is not attained, microtrauma following coughing for example, will repeatedly trigger a foreign body response to the lung device. On the other hand, the unidirectional valve system depends on a free moving silicone duck-bill. This sets a threshold for cellularization, beyond which implant function can be impaired. Hence, the same proteins that may conform beneficial tissue integration in subcutaneous implants, could also impair the function of the valve in the airway.

Further investigations of protein adhesion and cellularization of devices with patient controls and an *in vitro* model would contribute to the characterization of biological responses to biomaterials implanted within the lungs. Through analysis of the biological and clinical characteristics of patients receiving lung implants, predictor-based models for lung implant therapy may be created. Findings from this research line will guide future lung implant design and clinical guidelines for material-based treatment.

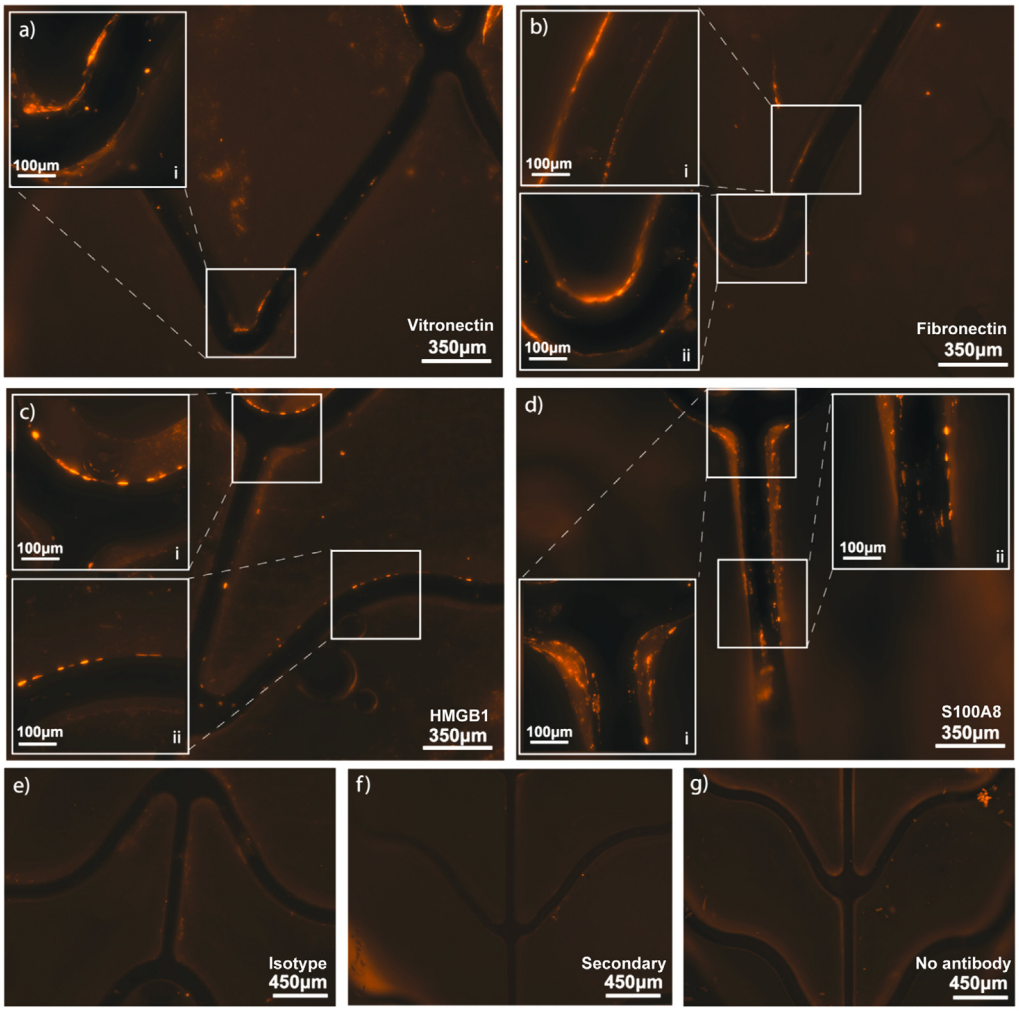

Fig. 6. Immunohistochemical validation of candidate extracellular matrix proteins and damage associated molecular patterns identified through LC-MS to be mutually adsorbed on the surface of endobronchial valves. Explanted endobronchial valves were stained with anti-vitronectin n=4 (a), anti-fibronectin n=4 (b), anti-HMGB1 n=2 (c), and anti-S100A8 n=2 (d) antibodies. White boxes, labeled as (i) and (ii) indicate sections with a greater magnification for better illustration. Rabbit IgG isotype n=2 (e), secondary antibody only n=4 (f) and no antibody staining n=3 (g) controls are shown. n = # of explanted valves stained.

5. Conclusion

The findings of this study have demonstrated that an MS-based discovery proteomics analysis of the proteins adsorbed on implant surfaces can provide meaningful biological insight into the interaction between a biomaterial and the lung. We have additionally identified several adhered proteins and associated biological pathways that may be responsible for an abnormal wound healing response to implantable lung devices, including DAMPs and ECM components. These findings set the groundwork for hypothesis generation and further exploration of the cellular and molecular mechanisms contributing to pathological wound healing around lung implants.

Declaration of Competing Interest

The authors declare the following financial interests/personal relationships which may be considered as potential competing interests:

Simon D. Pouwels and Dirk-Jan Slebos received funding from PulmonX Corp, USA. All other authors have nothing to disclose.

Acknowledgments

Part of the work has been performed in the UMCG Microscopy and Imaging Center (UMIC) under supervision of Prof. Dr. Ben N.G. Giepmans. This study was partly sponsored by ZonMW grant 91111.006.

References

[1] W.W. Montgomery, T-tube tracheal stent, Arch. Otolaryngol. - Head Neck Surg. 82 (3) (1965) 320–321.
[2] H. Dutau, D. Breen, A. Bugalho, L. Dalar, J. Daniels, C. Dooms, R. Eberhardt, L. Ek, M. Encheva, M. Febvre, M. Hackl, S. Marran, Z. Papai-Szekely, M. Perch, M. Roglic, A. Rosell, A. Rozman, P.L. Shah, M. Simon, A. Szlubowski, G. Stratakos, A. Sundset, T. Uibu, C. Von Garnier, B. Zaric, M. Zdraveska, L. Zuccatosta, D. Bokan, S. Arshad Husain, S. Bilaceroglu, P. Gasche-Soccal, S. Gasparini, F.J.F. Herth, M. Munavvar, Current practice of airway stenting in the adult population in Europe: a survey of the European association of bronchology and interventional pulmonology (EABIP), Respiration 95 (1) (2017) 44–54.
[3] K. Klooster, N.H.T. ten Hacken, J.E. Hartman, H.A.M. Kerstjens, E.M. van Rikxoort, D.-J. Slebos, Endobronchial valves for emphysema without interlobar collateral ventilation, N. Engl. J. Med. 373 (24) (2015) 2325–2335.
[4] D. Fallahi, H. Mirzadeh, M.T. Khorasani, Physical, mechanical, and biocompatibility evaluation of three different types of silicone rubber, J. Appl. Polym. Sci. 88 (10) (2003) 2522–2529.
[5] S.A. Shabalovskaya, Surface, corrosion and biocompatibility aspects of Nitinol as an implant material, BioMed. Mater. Eng. 12 (2002) 69–109.

[6] P.L. Shah, F.J. Herth, W.H. van Geffen, G. Deslee, D.-J. Slebos, Lung volume reduction for emphysema, Lancet Respir. Med. 5 (2) (2017) 147–156.
[7] N. Guibert, H. Saka, H. Dutau, Airway stenting: Technological advancements and its role in interventional pulmonology, Respirology 25 (9) (2020) 953–962.
[8] P.L. Shah, D.J. Slebos, Bronchoscopic interventions for severe emphysema: where are we now? Respirology 25 (9) (2020) 972–980.
[9] T.D. Koster, K. Klooster, N.H.T. Ten Hacken, M. van Dijk, D.-J. Slebos, Endobronchial valve therapy for severe emphysema: an overview of valve-related complications and its management, Expert Rev. Respir. Med. 14 (12) (2020) 1235–1247.
[10] Y. Bi, J. Li, L. Bai, X. Han, J. Ren, Long-term outcomes of tracheal stents removal under fluoroscopy guidance: comparison of tracheal fistulas and tracheal stenosis, BMC Pulmon. Med. 21 (1) (2021).
[11] F.T. Chung, S.M. Lin, C.L. Chou, H.C. Chen, C.Y. Liu, C.T. Yu, H.P. Kuo, Factors leading to obstructive granulation tissue formation after Ultraflex stenting in benign tracheal narrowing, Thorac. Cardiovasc. Surg. 58 (02) (2010) 102–107.
[12] J.M. Anderson, A. Rodriguez, D.T. Chang, Foreign body reaction to biomaterials, Semin. Immunol. 20 (2) (2008) 86–100.
[13] S.A. Roodenburg, S.D. Pouwels, D.-J. Slebos, Airway granulation response to lung-implantable medical devices: a concise overview, Eur. Respir. Rev. 30 (161) (2021) 210066.
[14] R. Klopfleisch, F. Jung, The pathology of the foreign body reaction against biomaterials, J. Biomed. Mater. Res. Part A 105 (3) (2016) 927–940.
[15] P. de Boer, N.M. Pirozzi, A.H.G. Wolters, J. Kuipers, I. Kusmartseva, M.A. Atkinson, M. Campbell-Thompson, B.N.G. Giepmans, Large-scale electron microscopy database for human type 1 diabetes, Nat. Commun. 11 (1) (2020).
[16] H. Heberle, G.V. Meirelles, F.R. da Silva, G.P. Telles, R. Minghim, InteractiVenn: a web-based tool for the analysis of sets through Venn diagrams, BMC Bioinf. 16 (1) (2015).
[17] U. Raudvere, L. Kolberg, I. Kuzmin, T. Arak, P. Adler, H. Peterson, J. Vilo, g:Profiler: a web server for functional enrichment analysis and conversions of gene lists (2019 update), Nucleic Acids Res. 47 (W1) (2019) W191–W198.
[18] J. Reimand, R. Isserlin, V. Voisin, M. Kucera, C. Tannus-Lopes, A. Rostamianfar, L. Wadi, M. Meyer, J. Wong, C. Xu, D. Merico, G.D. Bader, Pathway enrichment analysis and visualization of omics data using g:Profiler, GSEA, Cytoscape and EnrichmentMap, Nat. Protoc. 14 (2) (2019) 482–517.
[19] P. Shannon, Cytoscape: a software environment for integrated models of biomolecular interaction networks, Genome Res. 13 (11) (2003) 2498–2504.
[20] D. Merico, R. Isserlin, O. Stueker, A. Emili, G.D. Bader, Enrichment map: a network-based method for gene-set enrichment visualization and interpretation, PLoS One 5 (11) (2010) e13984.
[21] J.H. Morris, L. Apeltsin, A.M. Newman, J. Baumbach, T. Wittkop, G. Su, G.D. Bader, T.E. Ferrin, clusterMaker: a multi-algorithm clustering plugin for Cytoscape, BMC Bioinf. 12 (1) (2011).
[22] M. Kucera, R. Isserlin, A. Arkhangorodsky, G.D. Bader, AutoAnnotate: A Cytoscape app for summarizing networks with semantic annotations, F1000Research 5 (2016) 1717.
[23] L. Oesper, D. Merico, R. Isserlin, G.D. Bader, WordCloud: a Cytoscape plugin to create a visual semantic summary of networks, Source Code Biol. Med. 6 (1) (2011).
[24] X. Shao, I.N. Taha, K.R. Clauser, Y. Gao, A. Naba, MatrisomeDB: the ECM-protein knowledge database, Nucleic Acids Res. 48 (D1) (2019) D1136–D1144.
[25] C.W. Frevert, J. Felgenhauer, M. Wygrecka, M.V. Nastase, L. Schaefer, Danger-associated molecular patterns derived from the extracellular matrix provide temporal control of innate immunity, J. Histochem. Cytochem. 66 (4) (2018) 213–227.
[26] J.S. Roh, D.H. Sohn, Damage-associated molecular patterns in inflammatory diseases, Immune Netw. 18 (4) (2018).
[27] J. Zindel, P. Kubes, DAMPs, PAMPs, and LAMPs in immunity and sterile inflammation, Ann. Rev. Pathol. 15 (1) (2020) 493–518.
[28] J. Schindelin, I. Arganda-Carreras, E. Frise, V. Kaynig, M. Longair, T. Pietzsch, S. Preibisch, C. Rueden, S. Saalfeld, B. Schmid, J.-Y. Tinevez, D.J. White, V. Hartenstein, K. Eliceiri, P. Tomancak, A. Cardona, Fiji: an open-source platform for biological-image analysis, Nat. Methods 9 (7) (2012) 676–682.
[29] D.P. Franzen, C. Lang, N. Agorastos, L. Freitag, M. Kohler, P. Schmid-Grendelmeier, Evaluation of nickel release from endobronchial valves as a possible cause of hypersensitivity pneumonitis in a patient treated with bronchoscopic lung volume reduction, Int. Arch. Allergy Immunol. 174 (3–4) (2017) 144–150.
[30] J.P. Heggers, N. Kossovsky, R.W. Parsons, M.C. Robson, R.P. Pelley, T.J. Raine, Biocompatibility of Silicone Implants, Ann. Plast. Surg. 11 (1) (1983) 38–45.
[31] B.H. Shin, B.H. Kim, S. Kim, K. Lee, Y.B. Choy, C.Y. Heo, Silicone breast implant modification review: overcoming capsular contracture, Biomater. Res. 22 (1) (2018).
[32] Z. Othman, B. Cillero Pastor, S. van Rijt, P. Habibovic, Understanding interactions between biomaterials and biological systems using proteomics, Biomaterials 167 (2018) 191–204.
[33] M. Rahmati, E.A. Silva, J.E. Reseland, C.A. Heyward, H.J. Haugen, Biological responses to physicochemical properties of biomaterial surface, Chem. Soc. Rev. 49 (15) (2020) 5178–5224.
[34] B. Shen, M.K. Delaney, X. Du, Inside-out, outside-in, and inside–outside-in: G protein signaling in integrin-mediated cell adhesion, spreading, and retraction, Curr. Opin. Cell Biol. 24 (5) (2012) 600–606.
[35] R.M. Visalakshan, M.N. MacGregor, S. Sasidharan, A. Ghazaryan, A.M. Mierczynska-Vasilev, S. Morsbach, V. Mailänder, K. Landfester, J.D. Hayball, K. Vasilev, Biomaterial surface hydrophobicity-mediated serum protein adsorption and immune responses, ACS Appl. Mater. Interfaces 11 (31) (2019) 27615–27623.
[36] S.P. Barr, E.W. Hill, A. Bayat, Novel proteomic assay of breast implants reveals proteins with significant binding differences: implications for surface coating and biocompatibility, Aesthet. Surg. J. 38 (9) (2018) 962–969.
[37] B.R. Young, W.G. Pitt, S.L. Cooper, Protein adsorption on polymeric biomaterials I. Adsorption isotherms, J. Colloid Interface Sci. 124 (1) (1988) 28–43.
[38] D. Yang, X. Lü, Y. Hong, T. Xi, D. Zhang, The molecular mechanism of mediation of adsorbed serum proteins to endothelial cells adhesion and growth on biomaterials, Biomaterials 34 (23) (2013) 5747–5758.
[39] J. Andersson, K.N. Ekdahl, R. Larsson, U.R. Nilsson, B. Nilsson, C3 adsorbed to a polymer surface can form an initiating alternative pathway convertase, J. Immunol. 168 (11) (2002) 5786–5791.
[40] A. Faiz, M. van den Berge, C.J. Vermeulen, N.H.T. ten Hacken, V. Guryev, S.D. Pouwels, AGER expression and alternative splicing in bronchial biopsies of smokers and never smokers, Respir. Res. 20 (1) (2019).
[41] S.H. Haider, A. Oskuei, G. Crowley, S. Kwon, R. Lam, J. Riggs, M. Mikhail, A. Talusan, A. Veerappan, J.S. Kim, E.J. Caraher, A. Nolan, Receptor for advanced glycation end-products and environmental exposure related obstructive airways disease: a systematic review, Eur. Respir. Rev. 28 (151) (2019) 180096.
[42] S.J.M. Hoonhorst, A.T. Lo Tam Loi, S.D. Pouwels, A. Faiz, E.D. Telenga, M. van den Berge, L. Koenderman, J.-W.J. Lammers, H.M. Boezen, A.J.M. van Oosterhout, M.E. Lodewijk, W. Timens, D.S. Postma, N.H.T. ten Hacken, Advanced glycation endproducts and their receptor in different body compartments in COPD, Respir. Res. 17 (1) (2016).
[43] K.A. Sanders, D.A. Delker, T. Huecksteadt, E. Beck, T. Wuren, Y. Chen, Y. Zhang, M.W. Hazel, J.R. Hoidal, RAGE is a critical mediator of pulmonary oxidative stress, alveolar macrophage activation and emphysema in response to cigarette smoke, Sci. Rep. 9 (1) (2019).
[44] S.D. Pouwels, I.H. Heijink, N.H. ten Hacken, P. Vandenabeele, D.V. Krysko, M.C. Nawijn, A.J. van Oosterhout, DAMPs activating innate and adaptive immune responses in COPD, Mucosal Immunol. 7 (2) (2013) 215–226.
[45] L.A. McKiel, L.E. Fitzpatrick, Toll-like receptor 2-dependent NF-κB/AP-1 activation by damage-associated molecular patterns adsorbed on polymeric surfaces, ACS Biomater. Sci. Eng. 4 (11) (2018) 3792–3801.
[46] D.R. Schmidt, H. Waldeck, W.J. Kao, in: Protein Adsorption to Biomaterials, Biological Interactions on Materials Surfaces, Springer, US, 2009, pp. 1–18.
[47] M.-N. Abdallah, S.D. Tran, G. Abughanam, M. Laurenti, D. Zuanazzi, M.A. Mezour, Y. Xiao, M. Cerruti, W.L. Siqueira, F. Tamimi, Biomaterial surface proteomic signature determines interaction with epithelial cells, Acta Biomater. 54 (2017) 150–163.